BIOLOGY OF REPRODUCTION **81,** 1196–1205 (2009)
Published online before print 26 August 2009.
DOI 10.1095/biolreprod.109.078980

Rat *hd* Mutation Reveals an Essential Role of Centrobin in Spermatid Head Shaping and Assembly of the Head-Tail Coupling Apparatus[1]

František Liška,[2,4,5] Claudia Gosele,[5] Eugene Rivkin,[6] Laura Tres,[6] M. Cristina Cardoso,[3,5] Petra Domaing,[5] Eliška Krejčí,[7] Pavel Šnajdr,[7] Min Ae Lee-Kirsch,[8] Dirk G. de Rooij,[9,10] Vladimír Křen,[4] Drahomíra Křenová,[4] Abraham L. Kierszenbaum,[6] and Norbert Hubner[5]

Institute of Biology and Medical Genetics,[4] First Faculty of Medicine, Charles University in Prague, Praha, Czech Republic
Max-Delbrück-Center for Molecular Medicine,[5] Berlin, Germany
Department of Cell Biology and Anatomy,[6] The Sophie Davis School of Biomedical Education, New York, New York
Institute of Anatomy,[7] First Faculty of Medicine, Charles University in Prague, Praha, Czech Republic
Department of Pediatrics,[8] Technical University Dresden, Dresden, Germany
Center for Reproductive Medicine,[9] Academic Medical Center, Amsterdam, The Netherlands
Department of Endocrinology and Metabolism,[10] Utrecht University, Utrecht, The Netherlands

ABSTRACT

The hypodactylous (*hd*) locus impairs limb development and spermatogenesis, leading to male infertility in rats. We show that the *hd* mutation is caused by an insertion of an endogenous retrovirus into intron 10 of the *Cntrob* gene. The retroviral insertion in *hd* mutant rats disrupts the normal splicing of *Cntrob* transcripts and results in the expression of a truncated protein. During the final phase of spermiogenesis, centrobin localizes to the manchette, centrosome, and the marginal ring of the spermatid acroplaxome, where it interacts with keratin 5-containing intermediate filaments. Mutant spermatids show a defective acroplaxome marginal ring and separation of the centrosome from its normal attachment site of the nucleus. This separation correlates with a disruption of head-tail coupling apparatus, leading to spermatid decapitation during the final step of spermiogenesis and the absence of sperm in the epididymis. *Cntrob* may represent a novel candidate gene for presently unexplained hereditary forms of teratozoospermia and the "easily decapitated sperm syndrome" in humans.

acroplaxome, centrobin, centrosome, spermatid, spermatogenesis, teratozoospermia

INTRODUCTION

Spermatogenesis is a highly complex process involving the differentiation of spermatogonia into sperm. After meiosis, round haploid spermatids undergo elongation of the nucleus and condensation of the chromatin accompanied by a replacement of somatic histones by protamines bound to DNA, as well as formation of the acrosome and the flagellum. One of the major causes of male infertility is the abnormal development of spermatids into motile sperm. Defects in sperm development can cause various types of teratozoospermia associated with deformations of the head (e.g., globozoospermia, or round-headed sperm) and coiled sperm tails. These abnormalities have been associated with defective acrosome biogenesis and a disruption of the intramanchette and intraflagellar transport of protein cargos [1]. During acrosome biogenesis, Golgi-derived proacrosomal vesicles tether to the acroplaxome, a cytoskeletal plate that anchors the acrosome to the spermatid nuclear envelope [2]. The acroplaxome consists of an F-actin/keratin 5-containing plate bordered by a desmosomelike marginal ring fastening the descending recess of the acrosome to the spermatid nuclear envelope. The transient microtubule-containing manchette develops caudally to the acrosome-acroplaxome complex and surrounds the posterior half of the elongating spermatid nucleus. The perinuclear ring, the insertion site of manchette microtubules, assembles caudally and closely associated to the marginal ring of the acroplaxome. The marginal ring consists of two plaques: an acrosome-dense plaque with an associated bundle of keratin 5-containing intermediate filament, and a juxtaposed nuclear plaque firmly attached to the spermatid nuclear envelope [2]. A structural and biochemical analysis of several mouse mutants with spermatid head-shape abnormalities (*azh*, *Hrb*, and *Gopc*) has led to the hypothesis that the acrosome-acroplaxome-manchette (AAM) complex plays a significant role in spermatid head shaping [3]. Although several molecular components of the AAM complex have been identified [4–6], details of the mechanism of spermatid head shaping remain to be determined.

Rats that are homozygous at the *hd* (hypodactyly; Entrez Gene ID: 24442) locus show a reduction of the digital arch and male infertility due to impaired spermatogenesis. The +/*hd* heterozygotes possess normal spermatogenesis and have normal limb development. [7]. Sperm from the *hd*/*hd* mutant resemble a type of (oligo)teratoasthenospermia in humans, with

[1]Supported in part by Czech Science Foundation grant nos. 301/07/P178 to F.L. and 304/06/0116 to D.K.; European Union grant nos. LSGH-2004-005235 and LSHG-CT-2005-019015 to N.H.; German Ministry for Science and Education grant no. NGFN2 to N.H.; Ministry of Education, Youth and Sports of the Czech Republic grant no. MSM0021620806 to P.S.; and National Institutes of Health grant nos. HD36477 to L.T. and HD37282 to A.L.K.
[2]Correspondence: František Liška, Charles University in Prague, First Faculty of Medicine, Institute of Biology and Medical Genetics, Albertov 4, 128 00 Praha 2, Czech Republic. FAX: 420 224 918 666; e-mail: frantisek.liska@lf1.cuni.cz
[3]Current address: Department of Biology, Technische Universität Darmstadt, Schnittspahnstrasse 10, 64287 Darmstadt, Germany.

Received: 22 May 2009.
First decision: 24 June 2009.
Accepted: 29 July 2009.

eISSN: 1529-7268 http://www.biolreprod.org
ISSN: 0006-3363

marked sperm tail fragility and decapitated sperm heads [8–10]. Using linkage mapping, we have previously shown [11] that the rat *hd* locus is distinct from mouse *Hd* [12], which in contrast to the *hd* rats does not show spermatogenesis impairment.

Here, we report that the *hd* locus contains the insertion of an endogenous retrovirus (ERV-K8e family), resulting in the inactivation of *Lip8* gene. Tchernev et al. [13] identified by yeast two-hybrid screening this gene as *Lip8* (for LYST [lysosomal trafficking regulator]-interacting protein 8). Subsequently, Zou et al. [14], searching for BRCA2 interactors by yeast two-hybrid screening, found the same gene, which they named centrobin (*CNTROB*) because of the centriolar association of the encoded protein. Recent work has identified LIP8/centrobin as NIP2 (Nek2-interacting protein 2) [15], with a potential role in microtubule stabilization and mediated by NIP2 phosphorylation by Nek2 protein kinase. Knockdown of NIP2 in cultured cells led to inhibition of centriole duplication and resulted in centrosomes with one or no centrioles. In addition, microtubule assembly defects and abnormal nuclear morphology were observed [15]. In this paper, the designation *Cntrob* is used for the gene (Entrez Gene ID: 303240; Rat Genome Database ID: 1307488), and centrobin is used for the encoded protein. We provide evidence that centrobin is a structural component of the marginal ring of the spermatid acroplaxome, the manchette, and the head-tail coupling apparatus (HTCA), and that centrobin and keratin 5 interact with each other.

MATERIALS AND METHODS

Animals and Positional Cloning

All animal experiments were approved by The Charles University Animal Care Committee. The *hd* is propagated as Wistar hypodactylous (WHD) strain by brother-sister mating of *hd*/*hd* females with (fertile) +/*hd* males. Congenic BN-*hd* and SHR-*hd* rats were derived by cross-intercross mating of hypodactylous WHD females to BN/Cub or SHR males, respectively, using marker-assisted selection. The phenotype was assessed by the presence of hypodactyly and male infertility based on unsuccessful mating or dissection of the reproductive tract and inspection of cauda epididymal sperm. Tail DNA was genotyped by PCR amplification of microsatellite markers selected from public databases or derived from the rat chromosome 10 sequence using Pompous [16]. Primer3 was used for primer design [17]. The linkage map was constructed using MapManager QTX [18] separately for BC, F(2), and congenic backcrosslike and intercrosslike families and merged manually to form an integrated map. The *hd* was fine-mapped directly in backcross and by homozygosity-content mapping [19] in intercross populations. The BAC contig was constructed by sequence-tagged site content using the RPCI-32 BAC library (http://bacpac.chori.org/). Candidate genes were sequenced either by RT-PCR from testis RNA or by PCR from genomic DNA using BigDye Terminator chemistry (ABI, Foster City, CA). GenBank accession numbers of genes sequenced in this study are in Supplemental Table S1 (all Supplemental Data are available at www.biolreprod.org). Genotyping of the *hd* allele was performed by PCR using a reverse primer in exon 11 of *Cntrob* and two forward primers in intron 10 and within the retroviral long-terminal repeat (LTR), resulting in differently sized amplicons for the wild-type (WT) and the *hd* allele, respectively. Partial *Cntrob* cDNA (exons 10 and 11) and full-length *Cntrob* cDNA were amplified from testicular RNA of an *hd*/*hd* rat and cloned into pDrive (PCR cloning kit; Qiagen, Hilden, Germany) and pCR-XL-TOPO (TOPO XL PCR Cloning Kit; Invitrogen, Carsbad, CA), respectively, and multiple clones were sequenced. In addition, a ~10-kb genomic fragment encompassing intron 10 was amplified using Takara LA Taq polymerase, cloned into pCR-XL-TOPO, and sequenced by primer walking.

Far Western Blot and Immunoprecipitation Analyses of Centrobin-Keratin 5 Interaction

Recombinant full-length centrobin was purified from *Escherichia coli* as described above. Generation of keratin 5 fusion protein and characterization of anti-keratin 5 serum have been reported previously [2]. Far Western blot analysis was performed as described previously [20]. Briefly, recombinant centrobin (110 kDa) and keratin 5 (40 kDa; amino acids 166–462) were fractionated on a 12% SDS-PAGE, transferred onto an Immobilon P membrane (Millipore, Billerica, MA), and prehybridized overnight at 4°C in PBS/0.1% Tween containing fetal calf serum. Membranes were incubated with keratin 5 and centrobin fusion proteins diluted 1:10 to 1:40 with ImmunoPure Gentle Ag/Ab Binding Buffer (Pierce [part of Thermo Fisher Scientific], Rockford, IL). Incubation of a duplicate blot with the dilution buffer alone served as a negative control. Blots were then incubated with anti-keratin 5 and anti-centrobin antibody, followed by alkaline phosphatase-conjugated anti-rabbit immunoglobulin G and developed using 5-bromo-4-chloro-3-indolyl phosphate/nitro blue tetrazolium (BCIP/NBT) substrate.

Coimmunoprecipitation of centrobin and keratin 5 was carried out as described previously [21] using affinity-purified antibodies to centrobin or keratin 5. Briefly, antibodies were bound to protein A-Sepharose CL-4B beads (Amersham, Piscataway, NJ) by rocking at 4°C for 1 h in RSB100 buffer (10 mM Tris, pH 7.4; 100 mM NaCl; and 2.5 mM $MgCl_2$) containing 0.5% Triton X-100 (RSBT). The antibody-coated beads were washed four times with the same buffer and incubated for 20 min with rat testis urea extracts. The beads were then washed four times with RSBT and once with RSB100. The SDS-PAGE sample buffer was added, and bound proteins were dissociated from the resin by boiling. Obtained eluates were analyzed by immunoblotting using anti-keratin 5 and anti-centrobin sera.

Indirect Immunofluorescence, Electron Microscopy, and Immunogold Electron Microscopy

All procedures, including preparation of spermatogenic cells from isolated seminiferous tubules as well as the production and characterization of anti-keratin 5 antibody, have been described in detail previously [2]. The following antibodies were used: monoclonal anti-γ-tubulin antibody (1:100; Sigma, St. Louis, MO), monoclonal anti-centrin 20H5 (1:100; provided by Dr. Jeffrey Salisbury, Mayo Clinic, Rochester, MN), and polyclonal anti-centrobin N-terminal antibody (1:25 to 1:50 for immunogold electron microscopy).

Additional Methods

Methods for antibody generation, Western blotting, immunohistochemistry, and bioinformatics are provided in Supplemental *Materials and Methods*.

RESULTS

Insertion of a Retrotransposon in Cntrob *Intron at the* hd *Locus*

We defined the chromosomal region harboring the *hd* locus by genetic mapping to a 0.14-cM interval spanning 464 kb on rat chromosome 10 (Supplemental Fig. S1A and Supplemental Table S2). To confirm the nonrecombinant interval on a physical level, we constructed a minimal tiling path BAC contig built of four BAC clones (Supplemental Fig. S1B). The region contained 16 protein-coding genes (Supplemental Fig. S1C and Supplemental Table S3), 12 of which were expressed in the testis. Sequencing of the coding sequence of these genes revealed several synonymous and nonsynonymous single-nucleotide polymorphism changes among different rat strains (Supplemental Fig. S1D). Only one sequence variant was present exclusively in the *hd*/*hd* rats. This variant was characterized by RT-PCR spanning exons 8–11 and 10–13 and identified the presence of about 300-bp elongated transcripts in *hd*/*hd* homozygotes and +/*hd* heterozygotes compared with WT animals (Fig. 1A). Long-range PCR of genomic DNA from *hd*/*hd* homozygotes spanning intron 10 showed that the variant was an 8 kilobase pair intronic insertion (Fig. 1B). Sequence analysis of this 8360-bp insertion revealed that it likely represents an integration of a retroviral element (Fig. 1, B and C). Sequencing of *hd*/*hd* cDNA confirmed transcription of five aberrant mRNA species carrying retrovirus-derived exons spliced into the *Cntrob* transcript between exons 10 and 11 (Fig. 1C). Translation of the transcripts of the *hd* allele is predicted to result in truncated centrobin proteins consisting of the N-terminal 476

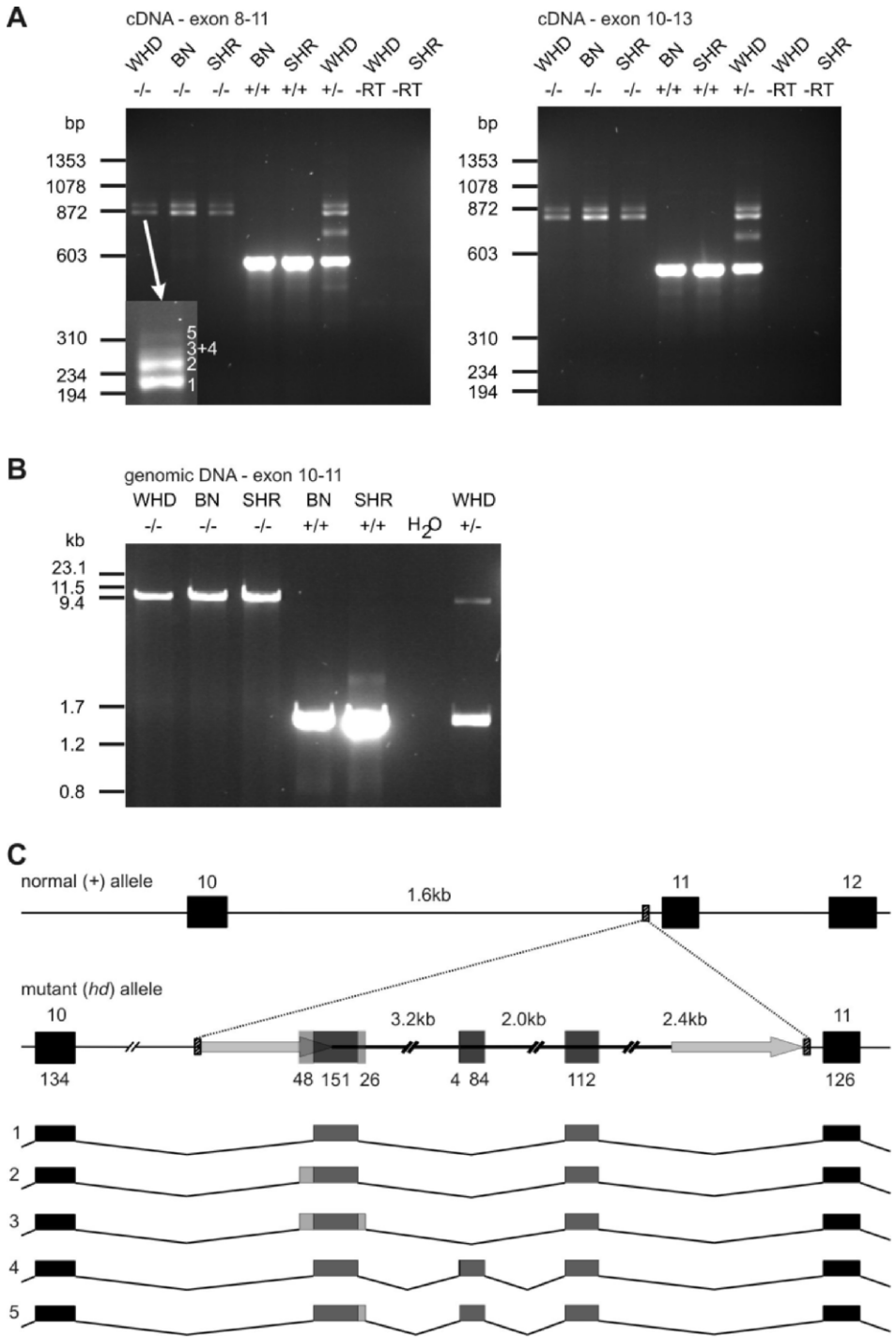

FIG. 1. Insertion of an endogenous retrovirus in intron 10 alters *Cntrob* transcription. The mutant allele symbol "*hd*" is replaced with "–" in **A** and **B**. Rat strains used were: Brown Norway (BN+/+), with the corresponding BN-*hd* congenic strain (BN–/–); spontaneously hypertensive rat (SHR+/+) with the corresponding SHR-*hd* congenic strain (SHR–/–); and Wistar hypodactylous WHD (–/–). **A**) The RT-PCR of *Cntrob* fragments with primers spanning exons 8–11 and exons 10–13 results in 564-bp and 518-bp products, respectively. Multiple amplicons derived from the *hd* (–/–) allele: two bright bands differing only slightly in length that are ~300 bp longer than the normal allele; there are also at least two faint bands that are even longer. This pattern is better recognizable in inset, showing a PCR product from the WHD mutant run for an extended period on a different gel. Numbers correspond to the expected mobility of alternative transcripts characterized in **C**. These amplicons were also seen in *hd* heterozygotes (+/–) but were absent in normal (+/+) rats. An additional band of ~700-bp mobility is seen among PCR products from heterozygote genomic DNA; it may represent a heteroduplex. –RT, negative control without reverse transcriptase. **B**) Long-range PCR from genomic DNA spanning exons 10 and 11 of *Cntrob* results in a ~10-kb product in *hd*/*hd* homozygotes (*hd*/*hd*) compared with the normal allele (1576 bp). The +/*hd* heterozygotes carry both alleles. H_2O, negative water control. **C**) Impact of retroviral insertion on genomic structure and transcription of *Cntrob*. The retrovirus inserts 40 bp upstream of exon 11 into a 6-bp sequence (GCTCCC; striped rectangle), which is duplicated in the *hd* allele as a result of the insertion (target site duplication; dotted line). The retroviral element (bold line) is flanked by identical LTR (arrows) and has a size of 7472 bp (not to scale). Five differently spliced mRNA species from the *hd*/*hd* mutants were identified by cloning of the mixture of RT-PCR products shown in **A**. *Cntrob* exons are indicated as black rectangles, and de novo retroviral exons are indicated as gray rectangles, with variable extensions in light gray. Accession numbers: EF532341, genomic DNA sequence of *hd*/*hd* mutants; the retrovirus insertion corresponds to nucleotide positions 303-8662; EF532346–50, five alternatively spliced cDNA sequences of *hd*/*hd* mutants; EF532342–45, cDNA sequences of four control rat strains.

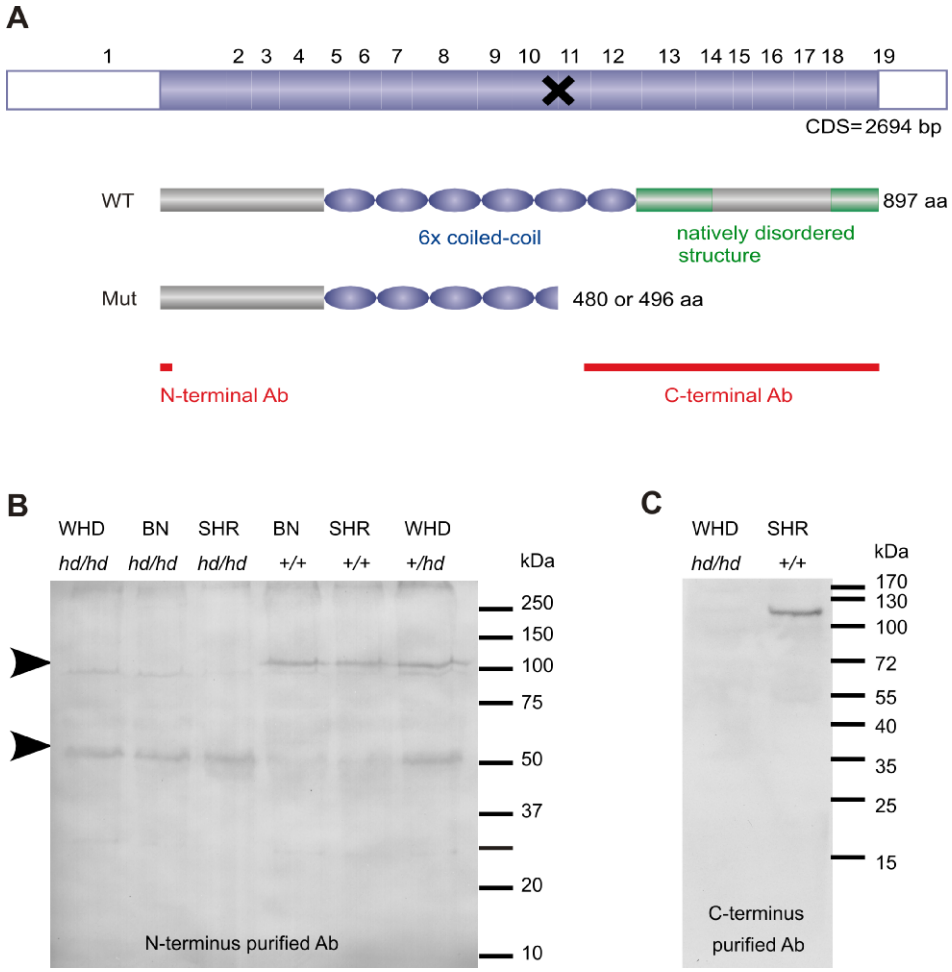

FIG. 2. Centrobin is truncated due to retrovirus insertion. **A**) Structure of *Cntrob* mRNA with 19 exons marked as filled (coding) and open (5′ and 3′ UTR) boxes. The "X" indicates retroviral insertion. Normal centrobin (WT) consists of an N-terminal domain with non-α, non-β secondary structure (gray) followed by six coiled-coil domains (violet ovals) and a C-terminal domain with disordered structure (green boxes). The entire C-terminal domain and two coiled-coils are missing in the mutant protein (Mut). Red bars indicate the antigen recognized by the N-terminal and C-terminal antibodies. **B**) Western blot analysis of testicular lysates using the anti-centrobin N-terminal antibody. WHD and two congenic *hd/hd* homozygotes are compared to WT controls (+/+) and a +/*hd* WHD heterozygote. Arrowheads at 110 kDa and 55 kDa indicate positions of WT and mutant centrobin. **C**) The antibody against the C terminus of centrobin (amino acids 530–897) detects only WT but not the truncated mutant form. Each lane in **B** and **C** was loaded by testis lysate containing 75 μg of proteins, as determined by Bradford assay.

amino acids followed by 4 or 20 insertion-derived amino acids and a premature stop codon (Fig. 2A and Supplemental Fig. S3A).

Centrobin Protein is Truncated in hd/hd *Rats*

Centrobin is highly conserved among mammals as well as in vertebrates (Supplemental Fig. S2). Computational structural analysis of centrobin, which has no similarity to other known proteins, predicted a central coiled-coil domain (amino acids 190–560) flanked by an N-terminal non-α, non-β secondary structure and two areas of highly disordered structure at the C terminus. The truncation of the protein in the *hd* mutant removes the C-terminal domain and approximately two of the six coiled-coils (Fig. 2A).

Western blot analysis using a polyclonal antibody against a peptide corresponding to the N terminus (amino acids 7–21) of centrobin revealed a protein of 110 kDa in normal testis, consistent with the predicted molecular mass, that was absent in mutant *hd/hd* homozygotes (Fig. 2B). A protein with a lower molecular mass close to 55 kDa was detected in *hd/hd* homozygotes, whereas both bands were seen in +/*hd* heterozygous animals, indicating that the low-molecular mass band represents the mutant truncated protein (Fig. 2B). The N-terminal antibody was specific, as demonstrated by competition with the corresponding peptide (Supplemental Fig. S3B). Furthermore, an antibody raised against the C-terminal 368 amino acids of centrobin recognized only the full-length protein, not the truncated form lacking the C terminus (Fig. 2C).

Centrobin, alternatively known as NIP2, is a centrosomal protein associated with daughter centrioles [14, 15, 22]; it has also been implicated in microtubule stabilization [15]. Indeed, we were able to confirm centrosomal localization of centrobin in normal fibroblasts (Supplemental Fig. S4A), whereas mutant *hd/hd*-derived fibroblasts showed a more diffuse cytoplasmic distribution with less-prominent centrosome localization (Supplemental Fig. S4, B and C). This finding is consistent with the proposed role of the C terminus for centriole targeting [14]. Despite the change in centrobin localization, the cell proliferation rate as well as the morphology of centrosomes and mitotic spindles in mutant fibroblasts were normal compared with normal controls (data not shown).

Localization of Centrobin in Developing Spermatids of Normal and hd/hd *Rats*

Spermiogenesis in *hd/hd* mutant males progressed undisturbed during the Golgi, cap, and acrosome phases of spermiogenesis. Yet, the number of spermatids decreased significantly (about 50%) during the final maturation phase, and the majority of elongating spermatids were found to be decapitated. Sperm were not present in the epididymal duct (data not shown).

In spermatocytes from normal rats, centrobin immunoreactivity colocalized with centrosomal γ-tubulin, thus indicating the presence of centrobin in the two centriolar components of the centrosome (Fig. 3, A–E). Elongating spermatids (step 14 of spermiogenesis [S14]) displayed centrobin-immunoreactive double dots at the attachment site of the developing tail to the

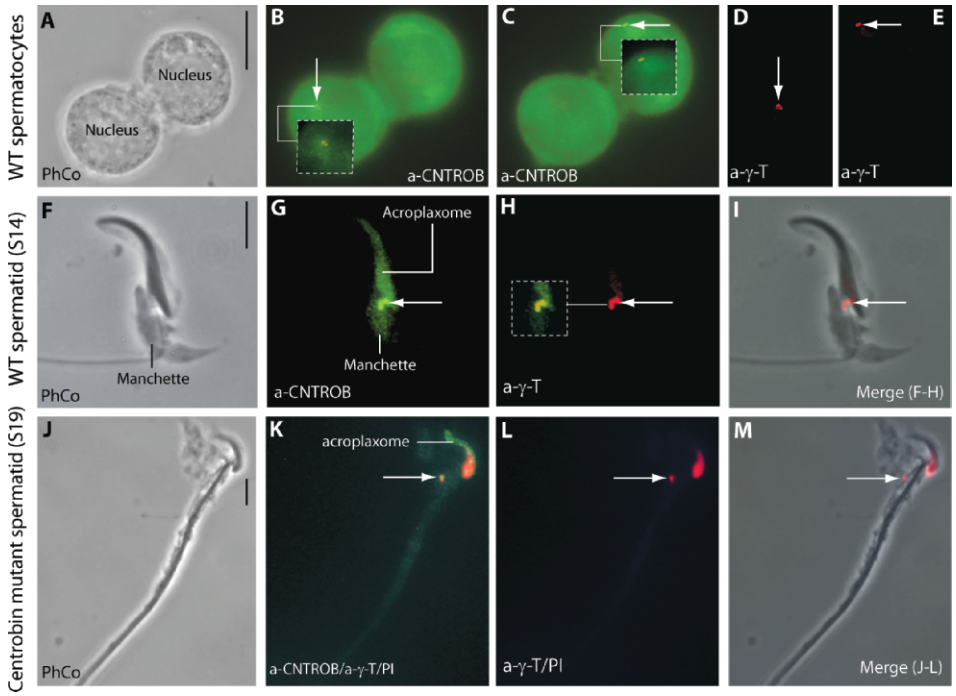

FIG. 3. Localization of centrobin in primary spermatocytes and spermatids. **A**) Phase-contrast microscopy (PhCo) of two conjoined primary spermatocytes collected from isolated spermatogenic, stage-specific seminiferous tubules of a WT rat. **B** and **C**) Arrows indicate centrobin immunofluorescent double dots corresponding to a centriolar pair. The dashed boxes in **B** and **C** denote merge images of the centrobin (green fluorescence)-γ-tubulin (red fluorescence; see **D** and **E**)-positive double dots. Note a slight shift in centrobin-γ-tubulin immunoreactivity. **F**) Phase-contrast microscopy of a WT elongating spermatid (S14). **G**) Arrow indicates centrobin immunofluorescent dots at the head-tail junction. The acroplaxome and manchette display centrobin immunoreactivity. A relatively weak immunoreactive signal in the manchette indicates that most centrobin has been transported to the centrosome region. **H**) Arrow indicates γ-tubulin-stained double dots. The dashed box denotes the merge image of centrobin-γ-tubulin-stained dots. Note a slight shift in the overlapping green (CNTROB)-stained and red (γ-tubulin)-stained dots. **I**) Arrow indicates the merged image of **F** and **H**, showing the juxtanuclear position of the centrosome. **J**) Phase-contrast microscopy of a mutant rat spermatid (S19). **K**) Merged image of anti-centrobin, anti-γ-tubulin, and propidium iodide (PI) fluorescence. γ-tubulin and PI signal alone is shown in **L**. Arrow indicates centrobin staining of just one centriolar component of the centrosome. The centrosome is not associated with the nucleus (stained red with propidium iodide [PI]). A slight shift in centrobin-γ-tubulin immunoreactivity is seen in the stained centriole. The acroplaxome is centrobin positive. **M**) Merge of **J** and **L**. Bar = 5 μm.

spermatid nucleus, where the centrioles of HTCA reside (Fig. 3, F–I). The staining of the distal dot was more intense than the one closely attached to the spermatid nucleus. A slight shift in the localization of centrobin with respect to γ-tubulin suggested a different distribution of these two proteins in the centrioles. In addition, weak centrobin immunoreactivity was also seen in the acroplaxome and the manchette (Fig. 3G). In contrast to spermatids from WT rats, a centrobin-immunoreactive centrosome in elongating spermatids of *hd*/*hd* rats was seen distant from the normal juxtanuclear site (Fig. 3, J–M). This observation was confirmed by electron microscopy (see below). Only one dot displayed combined centrobin and γ-tubulin immunoreactivity, thus suggesting that the other centriole was missing or that the specific immunoreactive sites were hidden. The characteristic slight shift in centriolar staining was apparent in the merged image (Fig. 3K). Centrobin staining in the acroplaxome persisted in mutants (Fig. 3K). The colocalization of centrobin and γ-tubulin in the centriolar pair of spermatocytes of the *hd*/*hd* mutant was comparable to spermatocytes of WT rats (data not shown).

Impairment of Intramanchette Transport in Centrobin Mutant Spermatids

Electron microscopy of S14 elongating spermatids of *hd*/*hd* rats revealed three significant alterations not observed in normal rat spermatids (Fig. 4A). First, the proximal centriole in spermatids was structurally normal but detached from the caudal nuclear region (Fig. 4B). This alteration was not seen in normal rat spermatids displaying a characteristically dense implantation site at the caudal nuclear boundary where HTCA attaches (Fig. 4A). In addition, the implantation density failed to develop at the caudal nuclear region (Fig. 4B). Second, the assembly of the perinuclear ring of the manchette was asymmetric and ectopic. Contrasting with the manchette encircling the elongating spermatid nucleus in normal spermatids (Fig. 4A), centrobin mutant spermatids exhibited a portion of the manchette perinuclear ring along the plasma membrane. The other portion of the ring retained its typical assembly and topographic features. Consequently, the arrangement of microtubule bundles emerging from each perinuclear ring portion was also asymmetric. Third, mitochondria and the material responsible for the assembly of the outer dense fibers of the developing tail were seen distributed in a disordered manner (Fig. 4C) instead of aligning along the developing axoneme as in normal S14 spermatids (compare with Fig. 4A). Collectively, these findings suggested a disturbance in the assembly of the manchette, leading to a possible disruption in the intramanchette transport of proteins to the HTCA and the developing tail. A defective intramanchette and intraflagellar transport was further supported by the dispersed deposit of outer dense fiber-like material (Fig. 4C) and the discontinuous fragmented pattern of α-tubulin immunoreactivity along the tails of relatively intact and decapitated spermatids (see below).

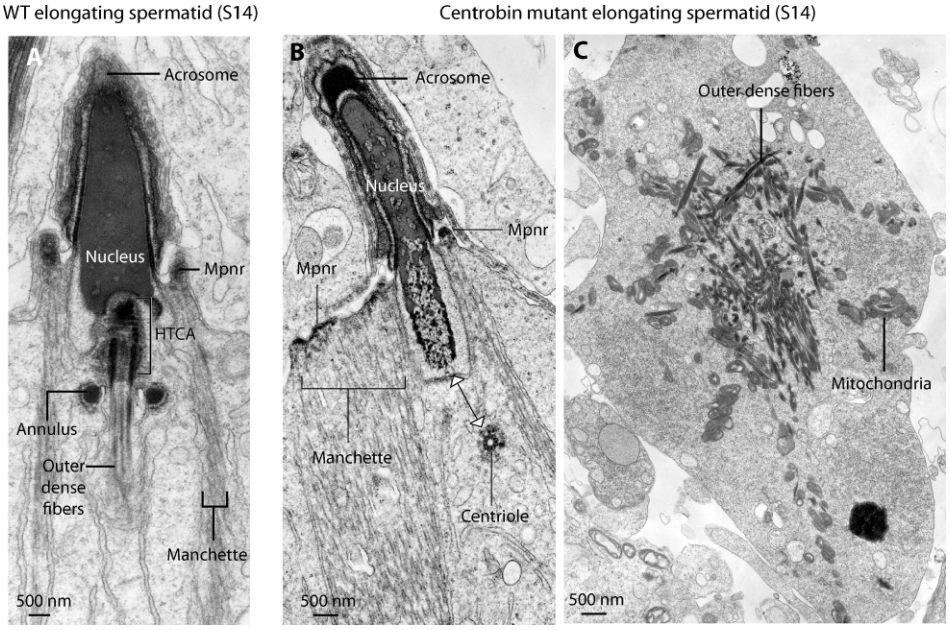

FIG. 4. Electron microscopy of S14 elongating spermatids of WT and *Cntrob* mutant. **A**) An S14 WT elongating spermatid shows components of the HTCA closely associated with the condensed nucleus that is capped by the acrosome. Outer dense fibers extending from the HTCA flank the axoneme of the developing tail. Microtubule bundles extend from the perinuclear ring of the manchette (Mpnr). The position of the annulus is indicated. **B**) An S14 spermatid from the *Cntrob* mutant displays a centriole separated from the usual nuclear attachment site by the distance denoted by the double-headed arrow. The Mpnr and emerging microtubules are ectopically asymmetric (compare with **A**). The apical (subacrosomal) condensation of the spermatid nucleus contrasts with the less-compact condensation at the opposite pole. **C**) The distal cytoplasm of an S14 spermatid of the *Cntrob* mutant contains dispersed outer dense fiber material and mitochondria. A corresponding phase-contrast microscopy view of a similar spermatid is shown in Figure 5M. Bar = 500 nm.

Centrobin Is Required for Structural Integrity of the Acroplaxome

To further examine the role of centrobin in spermatid head development, we analyzed its localization in the acroplaxome of round and elongating spermatids by immunofluorescence (Fig. 5, A–H) and electron microscopy (Fig. 5, I–L). In normal round spermatids, centrobin distributed diffusely in the acroplaxome plate and more prominently along its marginal ring (Fig. 5, A–D). The perinuclear ring of the manchette and the marginal ring of the acroplaxome aligned in parallel but were separated from each other by a narrow gap (Fig. 5, A–D). In normal elongating spermatids, centrobin immunoreactivity was seen in the acroplaxome as well as in the manchette (Fig. 5, E–H), thus suggesting an association of centrobin with the microtubular component of the manchette. In WT spermatids, the acroplaxome plate links the inner acrosomal membrane to the nuclear envelope. The marginal ring of the acroplaxome consists of two dense plaques: an acrosomal plaque, associated with the inner acrosomal membrane to which a bundle of keratin 5-containing filaments bind, and a nuclear plaque anchored to the spermatid nuclear envelope (Fig. 5I). Immunogold electron microscopy of normal spermatids showed a diffuse localization of centrobin along the acroplaxome plate and a prominent clustering at the acrosomal plaque (Fig. 5J). In contrast, the marginal ring of the acroplaxome in centrobin mutant spermatids revealed the absence of keratin 5-containing filaments normally anchored to the acrosomal plaque (Fig. 5K). In addition, elongating spermatids of *hd*/*hd* rats displayed several alterations: a vesicular segmentation of the acrosomal sac, an ectopic insertion of the perinuclear ring and associated microtubules of the manchette along the plasma membrane, constriction of the elongating spermatid nucleus at the site of the acroplaxome marginal ring, and vacuolization of the adjacent Sertoli cell cytoplasm (Fig. 5L). These abnormalities were not seen in WT rat spermatids (data not shown). We conclude that the ectopic position of the perinuclear ring of the manchette and the disproportionate constriction of the marginal ring of the acroplaxome, lacking keratin-5-containing filaments, contributed to an alteration in spermatid head shaping and defective intramanchette transport function. An ectopic buildup of α-tubulin was observed in elongating spermatids. Figure 5, M–P, shows a significant accumulation of α-tubulin immunoreactivity adjacent to the elongated spermatid head and at the margins of the caudal cytoplasm. Figure 5, Q–S, illustrates a discontinuous α-tubulin immunoreactive pattern along the tails of decapitated spermatids and tubulin aggregates in the residual head region devoid of its nuclear component. These observations suggested that the bulk of tubulin failed to be transported to the assembly sites and that the spermatid nuclear loss resulted in the formation of a tubulin-containing "shroud" at the tail decapitation site.

Centrobin Interacts with Keratin 5

The absence of keratin 5 filaments in mutant spermatids raised the possibility that these two proteins could interact directly or indirectly. To examine this further, we performed Far Western blot analysis [20] using recombinant centrobin and keratin 5 proteins. Western blots containing recombinant centrobin and keratin 5 were incubated with recombinant keratin 5 or centrobin, followed by detection with anti-keratin 5 or anti-centrobin antibodies. The anti-keratin 5 antibody did not cross-react with the 110-kDa band of centrobin (Fig. 6). However, prior incubation of the immobilized centrobin with keratin 5 led to cross-reaction of the 110-kDa band of centrobin with the anti-keratin 5 serum (Fig. 6A). Conversely, anti-centrobin cross-reacted with the band containing the blotted recombinant keratin 5 protein (40 kDa) only after prior incubation with centrobin (Fig. 6B). To delineate the location

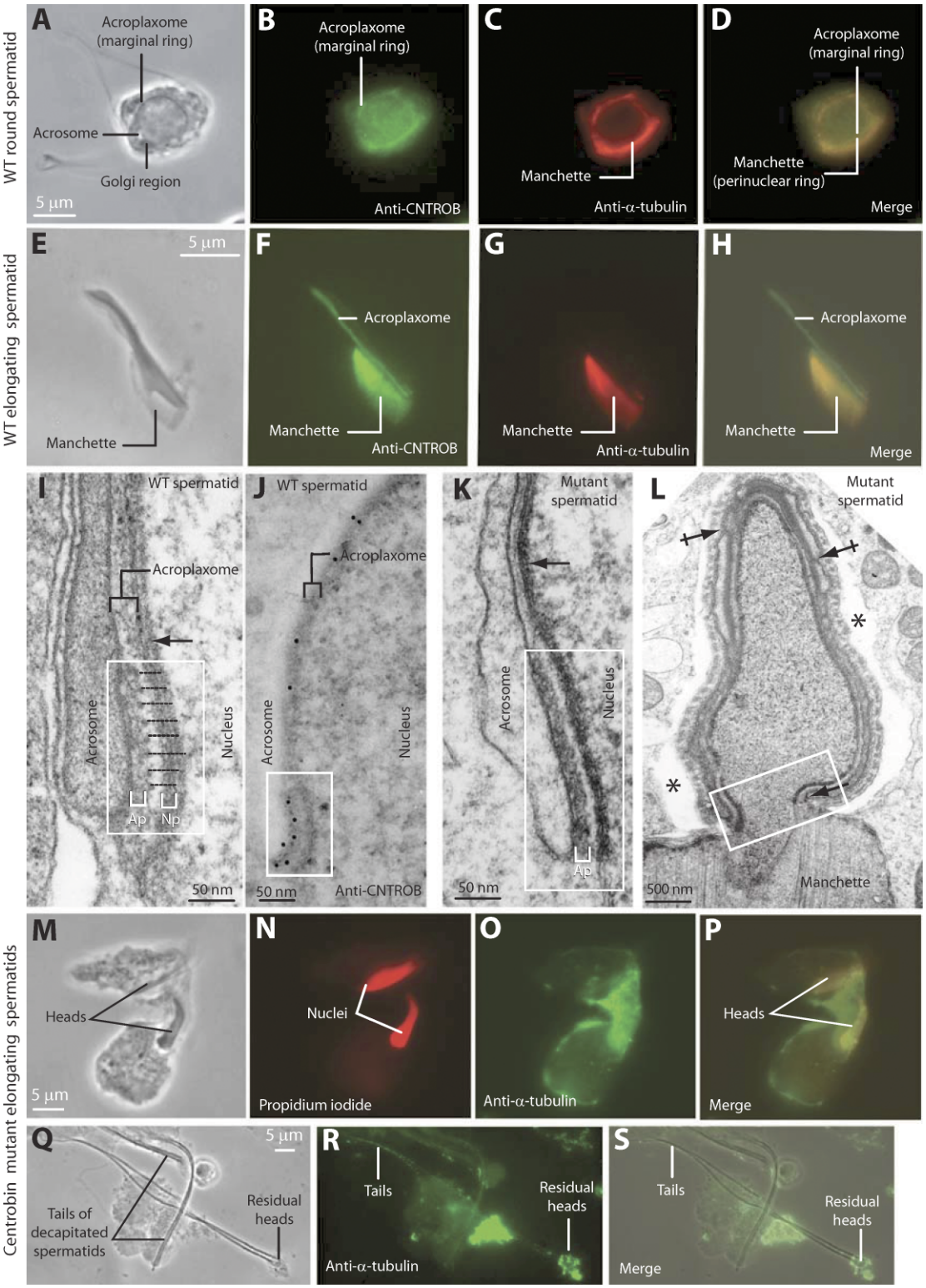

FIG. 5. Effects of the *Cntrob* mutation on acroplaxome structure. **A**) Phase-contrast microscopy of a round spermatid (S8) of a WT rat. **B**) Localization of centrobin in the acroplaxome plate and its marginal ring. **C**) Localization of α-tubulin within the manchette. **D**) Merge of **B** and **C** showing close apposition of the acroplaxome marginal ring (green) with the perinuclear ring of the manchette (red). **E**) Phase-contrast microscopy of an elongating spermatid (S12) of a WT rat. **F**) Centrobin immunofluorescence extends throughout the acroplaxome and the manchette. **G**) α-Tubulin staining of the manchette. **H**) Merge of **F** and **G**. **I**) Electron microscopy of the acroplaxome marginal ring (boxed) of a WT spermatid. Arrow indicates dense and thin nuclear lamina. Acrosomal plaque (Ap), a bundle of keratin 5-containing filament (indicated by the parallel lines), and nuclear plaque (Np) are denoted. **J**) Immunogold electron microscopy showing the localization of centrobin in the acroplaxome and the Ap region of the marginal ring. **K**) Electron microscopy of the marginal ring region of the acroplaxome of a *Cntrob* mutant rat. The Ap is well developed, keratin 5-containing filaments are absent, and the Np is poorly developed. The nuclear lamina (arrow) is visible. **L**) Electron microscopy of an elongating spermatid of a *Cntrob* mutant rat, indicating regressive late spermiogenesis. The caudal end of the nucleus is constricted at the level of the acroplaxome marginal ring (box). The perinuclear ring of the manchette and inserted microtubules are spread along the plasma membrane. Crossed arrows indicate segmentation of the acrosome. Asterisks indicate dilated Sertoli cell cisternae. **M**) Phase-contrast microscopy of two spermatid heads separated from their tail. A corresponding electron microscopy view of

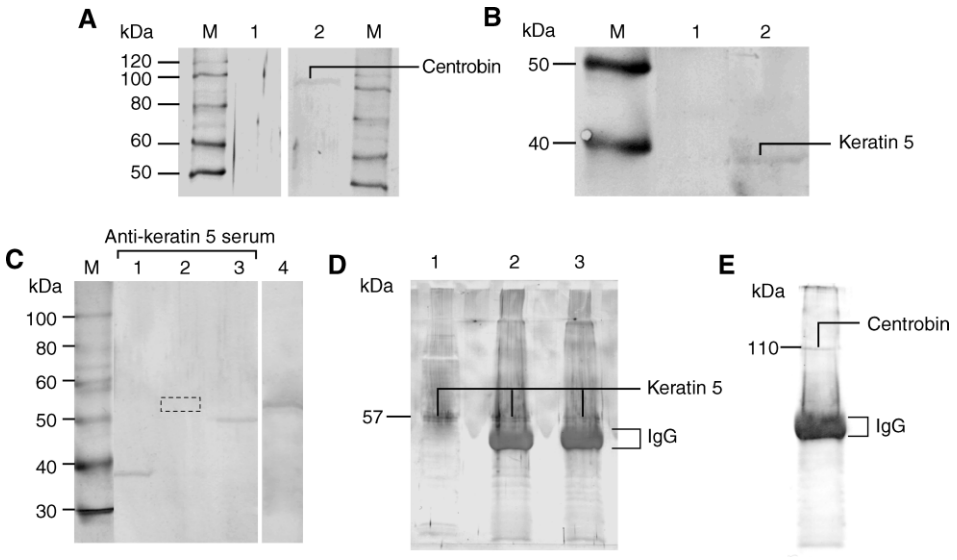

FIG. 6. Analysis of centrobin-keratin 5 interaction by far Western blotting and coimmunoprecipitation. **A**) Lane 1 (control) shows absence of cross-reactivity of anti-keratin 5 serum with the 110-kDa centrobin fusion protein. Lane 2 shows binding of anti-keratin 5 antibody to the 110-kDa centrobin protein after incubation of the blotted centrobin protein in a solution containing keratin 5 fusion protein. **B**) Centrobin antibody does not cross-react with the band containing keratin 5 fusion protein (lane 1, control) but binds to it after incubation with centrobin fusion protein (lane 2). **C**) Blot containing keratin 5 (lane 1), the N-terminal portion of centrobin (lane 2; expected position denoted by a dashed box), and the C-terminal portion of centrobin (lane 3) was incubated with keratin 5 fusion protein and developed using anti-keratin 5. Lane 4 is identical to lane 2 but developed using anti-centrobin (control). **D**) Testis extracts were incubated with anti-keratin 5. Lane 1 corresponds to the starting testis extract showing the 57-kDa keratin 5 protein. Lane 2 is a positive control. Lane 3 illustrates coimmunoprecipitated keratin 5 with anti-centrobin serum followed by immunoblotting. The blot was developed using anti-keratin 5 serum. **E**) The eluate from the coimmunoprecipitation experiment (shown in lane 3 **C**) contains centrobin protein (positive control) recognized by anti-centrobin. The molecular mass of the markers (M) is indicated in kDa in all the figures.

of the keratin 5-binding site on centrobin, we examined the binding of keratin 5 to recombinant N-terminal and C-terminal polypeptides of centrobin in a similar fashion. Figure 6C shows that keratin 5 binds to the C-terminal part (lane 3) but not to the N-terminal part (lane 2) of centrobin. To confirm that centrobin-keratin 5 binding also takes place in vivo, we performed coimmunoprecipitation experiments using testis extracts. Figure 6, D and E, shows that the incubation of testis extracts with anti-centrobin sera leads to the precipitation of both keratin 5 (Fig. 6D, lane 3) and centrobin (Fig. 6E, control) proteins, recognized by anti-K5 and anti-centrobin sera, respectively. Thus, these data provide evidence for a direct or indirect interaction of centrobin with keratin 5, supporting a role for centrobin in the assembly of the acroplaxome plate and its marginal ring in particular. It also may explain the negative effect in the *hd* mutant by eliminating the centrobin-binding site for keratin 5.

DISCUSSION

Insertion of an Endogenous Retrovirus into Cntrob *Gene Causes Truncation of the Centrobin Protein*

We have shown that the *hd* mutation in the WHD rat is caused by a mutagenic insertion of a retroviral element into intron 10 of the *Cntrob* gene on rat chromosome 10. Transcription of the *hd* allele gives rise to multiple mRNA species containing retrotransposon-derived exons that result in a C-terminally truncated centrobin protein. Centrobin has been implicated in the duplication of the centriole, and depletion of centrobin in HeLa cells is associated with lengthening of mitosis due to impaired cytokinesis [14]. In humans, centrobin is expressed in multiple tissues, with the highest expression seen in testis [14], indicating a role for centrobin in testicular function. Our data demonstrate the localization of centrobin in the centrosome of spermatocytes and spermatids and reveal that it is also present in the acroplaxome and its marginal ring and the manchette. We further establish that the C terminus is likely responsible for centrosomal targeting of centrobin in fibroblasts, because C-terminally truncated mutant centrobin distributes diffusely within the cytoplasm. This is supported by analysis of deletion mutants of *CNTROB* in HeLa and 293T cells [14, 15]. Regarding the importance of the centrosome for mitosis, and in light of a recent study showing a requirement of centrobin for spindle assembly during early embryogenesis [23], it is interesting that the *hd* mutant fibroblasts in cell culture did not show a proliferation defect. However, it is possible that the truncated centrobin may exert only slight or tissue-specific effects on proliferation. A subtle impairment of mitosis may be highly detrimental in fast-dividing embryonal limb bud mesenchyme and may hence underlie the limb deformity—hypodactyly—in *hd* mutants.

Centrobin Is Required for Development of the HTCA During Late Spermiogenesis

Although the C-terminally truncated centrobin fails to localize in fibroblast centrioles, it is clearly present in the

the cytoplasmic region of a similar spermatid is shown in Fig. 4C. **N**) Propidium iodide staining of the nuclei. **O**) Large aggregates of α-tubulin in the spermatid head. **P**) Merge of **N** and **O**. **Q**) Tails of decapitated spermatids, two of them caped by residual heads lacking their nuclei. **R**) A linear fragmented distribution of α-tubulin along the tails and a significant accumulation of α-tubulin in the residual heads devoid of nuclei. **S**) Merge of **Q** and **R**.

acroplaxome, manchette, and centrosome of *hd*/*hd* elongating spermatids. However, our results point to an abnormal function of truncated centrobin in the AAM complex in spermatids of the mutant. An acroplaxome-containing F-actin-keratin 5 network links the acrosome to the spermatid nuclear envelope. We show that centrobin is a structural component of the acroplaxome and its marginal ring, where the keratin 5-containing filament bundle assembles in close association with the desmosome-like acrosome plaque. It was reported previously that keratin 5 is not present in the acroplaxome of the *Hrb* mouse mutant displaying spherical sperm heads [24]. Therefore, the absence of keratin 5-containing filaments in the marginal ring of the acroplaxome in the *hd*/*hd* mutant may be related to a possible recruiting or scaffolding function of centrobin (alone or in complex with other proteins) that is impaired in the mutant rat lacking the C-terminal region of this protein. A similar mechanism may account for the failure of the HTCA to attach to the implantation fossa in the spermatid nucleus. A combined defect in the development of a functional acroplaxome marginal ring and the displacement of the HTCA from its normal nuclear attachment site may disrupt the head-tail connection, leading to spermatid decapitation during the final step of spermiogenesis, thus accounting for the absence of sperm in the epididymis. Centrobin is also present in the manchette, a transient microtubular structure that disassembles upon completion of spermatid head shaping. The manchette microtubules and associated F-actin filaments provide tracks for the intramanchette transport of cargos by molecular motors to the developing tail [1]. The finding of centrobin immunoreactivity in the manchette may reflect a role for centrobin in the intramanchette transport of protein cargos toward the developing HTCA. Alternatively, centrobin may also play a direct function in assembly and disassembly of the manchette. The latter possibility is in agreement with a role for the human centrobin ortholog in microtubule stabilization mediated by NIP2 phosphorylation by Nek2 protein kinase [15].

A relevant aspect in the *hd*/*hd* mutant rat is the decapitation of spermatids, leading to the absence of sperm in the epididymis. Additional significant observations are the deficient organization of the marginal ring of the acroplaxome, the constriction of the spermatid nucleus at the level of the marginal ring of the acroplaxome, and the ectopic assembly of the manchette. These structural changes occur during the shaping of the spermatid head, the organization and anchorage of the HTCA, and the development of the sperm tail. It is likely that a truncated centrobin protein may interfere with the normal completion of these three events. Whether centrobin alone or centrobin-associated proteins have a prominent role in the final steps of spermatid morphogenesis needs to be determined. It appears that an arrest in the completion of spermiogenesis triggers the collapse of the elongating spermatid population, demonstrated by the segmentation of the acrosome, decapitation, and a local vacuolization of the adjacent Sertoli cell at the Sertoli cell-spermatid interface, leading to the complete depletion of the spermatid progeny.

To our knowledge, this is the first report of a dysfunctional protein associated with sperm head decapitation, a frequent cause of infertility in men. The "detached tail" or "acephalic" phenotype, due to centrosome dysfunction, is a well-known cause of human male infertility and is thought to have a genetic origin [8]. Yet, the genetic factors contributing to this phenotype have not been characterized. Because in humans the centrioles are contributed exclusively to the zygote by the sperm, a failure of the centrosome to attach to the nucleus represents not only an obstacle to normal fertilization but also to intracytoplasmatic sperm injection [25]. Similarly to the somatic centrosome involved in the polarization of the mitotic spindle, the spermatid centrosome plays a comparable task in the polarized development of the sperm tail. In addition, the coexistence of centrobin in the acroplaxome and centrosome adds support to the hypothesis that the acroplaxome shares molecular components with the centrosome. An example is the presence in spermatids of the centrosome-associated protein ODF2 in the acroplaxome and the manchette [26].

The *hd* mutation yields a C-terminal truncation of centrobin protein. The truncated protein is still expressed but fails to attach to the centrioles in fibroblasts. In spermatogenic cells, the progression of mitosis (spermatogonia) and meiosis (spermatocytes) is not compromised until round spermatids. In elongating spermatids, truncated centrobin function may hamper the development of the AAM complex, leading to defective intramanchette transport of cargos essential for the organization and function of the HTCA. This possibility is supported by our finding that binding site for keratin 5 is located on the C-terminal part of centrobin, which is missing in centrobin *hd* mutants. It is interesting to note that the *hd* allele acts in strictly recessive fashion (heterozygotes are normal), so the truncated protein does not act as a dominant negative, despite its correct localization in spermatocytes, and in the detached centrosome, acroplaxome, and manchette of elongating spermatids. Most likely, the truncated protein represents a loss of function. However, we cannot exclude the possibility of a hypomorph. Thus, a complete absence of centrobin may lead to a different or even more pronounced phenotype, especially considering its potential role in microtubule stabilization during mitosis and in the manchette. A putative cytoskeletal scaffolding and transport function of centrobin may underlie both its role in centriole duplication control during cell division and centriole attachment to the spermatid nucleus. In summary, using a forward genetics approach in the rat, we have identified centrobin as a novel molecular component required for the structural integrity of the marginal ring of the acroplaxome, the correct assembly site of the HTCA, and possibly for the stabilization of manchette microtubules in rat spermatids. *Cntrob* may represent an interesting novel candidate gene for hereditary forms of teratozoospermia and the "easily decapitated sperm syndrome" in humans.

REFERENCES

1. Kierszenbaum AL. Intramanchette transport (IMT): managing the making of the spermatid head, centrosome, and tail. Mol Reprod Dev 2002; 63:1–4.
2. Kierszenbaum AL, Rivkin E, Tres LL. Acroplaxome, an F-actin-keratin-containing plate, anchors the acrosome to the nucleus during shaping of the spermatid head. Mol Biol Cell 2003; 14:4628–4640.
3. Kierszenbaum AL, Tres LL. The acrosome-acroplaxome-manchette complex and the shaping of the spermatid head. Arch Histol Cytol 2004; 67:271–284.
4. Mendoza-Lujambio I, Burfeind P, Dixkens C, Meinhardt A, Hoyer-Fender S, Engel W, Neesen J. The Hook1 gene is non-functional in the abnormal spermatozoon head shape (azh) mutant mouse. Hum Mol Genet 2002; 11: 1647–1658.
5. Mochida K, Tres LL, Kierszenbaum AL. Structural and biochemical features of fractionated spermatid manchettes and sperm axonemes of the azh/azh mutant mouse. Mol Reprod Dev 1999; 52:434–444.
6. Kierszenbaum AL, Tres LL. Bypassing natural sperm selection during fertilization: the azh mutant offspring experience and the alternative of spermiogenesis in vitro. Mol Cell Endocrinol 2002; 187:133–138.
7. Moutier R, Toyama K, Charrier MF. Hypodactyly, a new recessive mutation in the Norway rat. J Hered 1973; 64:99–100.
8. Chemes HE, Puigdomenech ET, Carizza C, Olmedo SB, Zanchetti F, Hermes R. Acephalic spermatozoa and abnormal development of the head-neck attachment: a human syndrome of genetic origin. Hum Reprod 1999; 14:1811–1818.
9. Kamal A, Mansour R, Fahmy I, Serour G, Rhodes C, Aboulghar M. Easily

decapitated spermatozoa defect: a possible cause of unexplained infertility. Hum Reprod 1999; 14:2791–2795.
10. Baccetti B, Capitani S, Collodel G, Di Cairano G, Gambera L, Moretti E, Piomboni P. Genetic sperm defects and consanguinity. Hum Reprod 2001; 16:1365–1371.
11. Křenová D, Pravenec M, Housa D, Liška F, Bílá V, Kašpárek R, Křen V. Linkage mapping of rat hypodactyly locus to chromosome 10. Transplant Proc 1999; 31:1620.
12. Post LC, Margulies EH, Kuo A, Innis JW. Severe limb defects in Hypodactyly mice result from the expression of a novel, mutant HOXA13 protein. Dev Biol 2000; 217:290–300.
13. Tchernev VT, Mansfield TA, Giot L, Kumar AM, Nandabalan K, Li Y, Mishra VS, Detter JC, Rothberg JM, Wallace MR, Southwick FS, Kingsmore SF. The Chediak-Higashi protein interacts with SNARE complex and signal transduction proteins. Mol Med 2002; 8:56–64.
14. Zou C, Li J, Bai Y, Gunning WT, Wazer DE, Band V, Gao Q. Centrobin: a novel daughter centriole-associated protein that is required for centriole duplication. J Cell Biol 2005; 171:437–445.
15. Jeong Y, Lee J, Kim K, Yoo JC, Rhee K. Characterization of NIP2/centrobin, a novel substrate of Nek2, and its potential role in microtubule stabilization. J Cell Sci 2007; 120:2106–2116.
16. Fondon JW III, Mele GM, Brezinschek RI, Cummings D, Pande A, Wren J, O'Brien KM, Kupfer KC, Wei MH, Lerman M, Minna JD, Garner HR. Computerized polymorphic marker identification: experimental validation and a predicted human polymorphism catalog. Proc Natl Acad Sci U S A 1998; 95:7514–7519.
17. Rozen S, Skaletsky H. Primer3 on the WWW for general users and for biologist programmers. Methods Mol Biol 2000; 132:365–386.
18. Manly KF, Cudmore RH Jr, Meer JM. Map Manager QTX, cross-platform software for genetic mapping. Mamm Genome 2001; 12:930–932.
19. Ward CJ, Hogan MC, Rossetti S, Walker D, Sneddon T, Wang X, Kubly V, Cunningham JM, Bacallao R, Ishibashi M, Milliner DS, Torres VE, Harris PC. The gene mutated in autosomal recessive polycystic kidney disease encodes a large, receptor-like protein. Nat Genet 2002; 30:259–269.
20. Edmondson DG, Roth SY. Identification of protein interactions by far Western analysis. Curr Methods Mol Biol 2001; 20:1–10.
21. Piñol-Roma S, Choi YD, Dreyfuss G. Immunological methods for purification and characterization of heterogeneous nuclear ribonucleoprotein particles. Methods Enzymol 1990; 181:317–325.
22. Andersen JS, Wilkinson CJ, Mayor T, Mortensen P, Nigg EA, Mann M. Proteomic characterization of the human centrosome by protein correlation profiling. Nature 2003; 426:570–574.
23. Sonn S, Jeong Y, Rhee K. Nip2/centrobin may be a substrate of Nek2 that is required for proper spindle assembly during mitosis in early mouse embryos. Mol Reprod Dev 2009; 76:587–592.
24. Kierszenbaum AL, Tres LL, Rivkin E, Kang-Decker N, van Deursen JM. The acroplaxome is the docking site of Golgi-derived myosin Va/Rab27a/b-containing proacrosomal vesicles in wild-type and Hrb mutant mouse spermatids. Biol Reprod 2004; 70:1400–1410.
25. Rawe VY, Terada Y, Nakamura S, Chillik CF, Olmedo SB, Chemes HE. A pathology of the sperm centriole responsible for defective sperm aster formation, syngamy and cleavage. Hum Reprod 2002; 17:2344–2349.
26. Rivkin E, Tres LL, Kierszenbaum AL. Genomic origin, processing and developmental expression of testicular outer dense fiber 2 (ODF2) transcripts and a novel nucleolar localization of ODF2 protein. Mol Reprod Dev 2008; 75:1591–1606.